Physics – Uspekhi **66** (5) 518 – 533 (2023)

INSTRUMENTS AND METHODS OF INVESTIGATION

PACS numbers: **28.60.+s**, **42.62.–b**, **87.56.–v**

Isotopically selective photoionization for the production of the medical radioisotope ^{177}Lu

A B Dyachkov, A A Gorkunov, A V Labozin, S M Mironov,
V A Firsov, G O Tsvetkov, V Ya Panchenko

DOI: https://doi.org/10.3367/UFNe.2021.12.039140

Contents

‘Abstract. We present results on isotopically selective lutetium photoionization using dye lasers pumped by copper vapor lasers as applied to the problem of obtaining the ^{177}Lu radionuclide for medical applications.

Keywords: selective photoionization, laser isotope separation, ^{177}Lu

1. Introduction

Lutetium is the last element of the lanthanide group. Natural lutetium consists of a mixture of stable ^{175}Lu with an abundance of 97.4% and weakly β-radioactive ^{176}Lu (half-life $T_{1/2} = 3.6 \times 10^{10}$ years) with a natural concentration of 2.6%. The remaining isotopes of lutetium (over 60, including isomers [1]) were obtained artificially and are radioactive with lifetimes from several milliseconds to several years. From an applied point of view, standing out among them is radioactive ^{177}Lu as the most requested medical radiopharmaceutical drug. Due to its nuclear-physical properties (a half-life of 6.7 days, a low average energy of β electrons ($\sim$ 133 keV), and a radius of impact on biological tissue of less than 2 mm), the isotope is considered the most suitable for the treatment of small tumors and metastases, having a minimal effect on healthy organs. The accompanying soft gamma radiation with energies of 113 and 208 keV makes possible diagnostics (visualization), dosimetric analysis, and optimization of the treatment process in each specific case, implementing the principles of personalized medicine.

Currently, there are two main methods for obtaining the ^{177}Lu isotope, which involve neutron irradiation of an isotopically enriched substance in a nuclear reactor. When ^{177}Lu is obtained by the indirect route, a target of highly enriched ^{176}Yb (natural concentration: 12.6%) is used, which, upon neutron capture, transforms into ^{177}Yb with further decay to form ^{177}Lu. The extraction of ^{177}Lu from the ytterbium carrier is performed by chemical methods. The concentration of the radionuclide isolated by this method reaches the theoretical limit of $\sim$ 100% [2, 3]; however, due to the small cross section for neutron capture by the ^{176}Yb nucleus (2.5 bn), a high neutron flux is required. Furthermore, during one irradiation session, only a small fraction of enriched ^{176}Yb ($\sim 10^{-4}$) transforms into ^{177}Lu, and the reuse of highly enriched ytterbium is difficult, which significantly increases the cost of the final product. The second method (direct route) harnesses the large cross section for neutron capture by the ^{176}Lu nucleus, approximately 2065 bn. In moderate neutron fluxes ($\sim 10^{14}$ cm^{-2} s^{-1}) when using highly enriched ^{176}Lu, the concentration of ^{177}Lu amounts to 20%, while with an intense neutron flux ($\sim 2 \times 10^{15}$ cm^{-2} s^{-1}) we can reach the level of 60% [4, 5]. A characteristic feature of this method, which distinguishes it from the previous one, is the presence in the irradiated product of a long-lived metastable nuclear isomer ^{177m}Lu with a half-life of 160 days. This difference in the lifetimes of the isomeric excited state and the ground state is due to the prohibition on dipole γ-ray transitions due to the large difference between nuclear spins: $I = 23/2$ for ^{177m}Lu and $I = 7/2$ for ^{177}Lu. The disadvantages of the direct method are the limited concentration of ^{177}Lu

A B Dyachkov, A A Gorkunov, A V Labozin, S M Mironov, V A Firsov, G O Tsvetkov (*), **V Ya Panchenko**
National Research Center Kurchatov Institute,
pl. Akademika Kurchatova 1, 123182 Moscow, Russian Federation
E-mail: (*) Tsvetkov_GO@nrcki.ru

Received 2 November 2021, revised 17 December 2021
Uspekhi Fizicheskikh Nauk **193** (5) 554 – 570 (2023)
Translated by E N Ragozin

and the presence of the ^{177m}Lu isomer, which leads to the formation of long-lived radioactive waste during the treatment of patients and presents certain problems during its storage and disposal. Recently, however, interest associated with the possibility of making a ^{177}Lu generator based on the nuclear transition of metastable ^{177m}Lu to the ground state [6] has also arisen in the extraction of the isomer itself. Due to the long lifetime of the isomer, such a generator could supply the medical industry with the ^{177}Lu radioisotope to the maximum extent for a long time, regardless of irradiation in a reactor.

In our work, we considered an alternative method for obtaining ^{177}Lu by isotope separation, based on the use of laser-induced isotopically selective photoionization of atoms. A feature of the method is the possibility of separating radioactive isotopes, since the main part of the installation — the laser system — does not undergo radioactive exposure. The theoretical and experimental foundations of the method, which have been known for over 50 years, are described in numerous publications [7–11]. We used laser photoionization to extract the ^{176}Lu isotope from natural lutetium for further irradiation and obtain ^{177}Lu by the direct method [12]. In Ref. [13], we proposed a method for obtaining ^{177}Lu, based on laser extraction of ^{177}Lu from natural metallic lutetium irradiated by neutrons. As a result of irradiation, the source material becomes a mixture of ^{175}Lu, ^{176}Lu, ^{177}Lu, and ^{177m}Lu isotopes. Depending on the intensity and duration of neutron irradiation, the ^{177}Lu concentration varies between 10^{-5} and 10^{-3}. Of these, approximately 10^{-3} atoms are long-lived isomers [14]. It is proposed to extract such small amounts of radioactive lutetium using selective laser photoionization. The sample is placed in a vacuum and evaporates at high temperature, forming a beam of atoms which passes through a laser-irradiated zone. Due to the isotopic uniqueness of the spectra of optical transitions, the radiation makes it possible to selectively ionize the ^{177}Lu isotope or the ^{177m}Lu isomer in order to further electrostatically separate photoions from a stream of neutral atoms, bypassing the stage of chemical purification from the remaining lutetium isotopes. The selectivity of ^{177}Lu photoionization with respect to ^{177m}Lu will make it possible to purify the radionuclide from the long-lived isomer and thus combine the advantages of the large activation cross section of the 'direct' method of obtaining the ^{177}Lu radionuclide from ^{176}Lu and the low isomer concentration characteristic of the 'indirect' method of obtaining ^{177}Lu from ^{176}Yb.

Mention should be made of three studies known to us that propose laser technologies for obtaining the ^{177}Lu radioisotope. Specifically, selective laser photoionization was used at the stage of enrichment of natural ytterbium with the isotope ^{176}Yb for the indirect method of obtaining ^{177}Lu [5]. The authors of [5] managed to increase the ytterbium concentration to more than 97% with a productivity of 27 mg h^{-1}. Reference [15] on laser separation of ytterbium isotopes in atomic vapor is also devoted to the development of enrichment technology. The preparation of effectively the ^{176}Yb monoisotope with a content of 99% from a natural mixture was demonstrated. In the production of weight quantities of 20 mg h^{-1}, the concentration reached 88% with the suppression of the amount of the ^{174}Yb isotope from 31.8% to 5%, the content of which is subject to severe restrictions for irradiation in the reactor. Another option for using laser technology for the production of ^{177}Lu pharmaceutical preparation is being developed by an international group at CERN at the CERN-MEDICIS facility [16, 17]. It is reported that two ways of producing the radioisotope are possible. The first involves the use of a 1.4 GeV proton beam from the CERN proton synchrotron. When protons interact with a target, isotopes of various chemical elements are produced, of which only lutetium isotopes are ionized in the laser field. The lutetium isotopes are then transported to an electromagnetic mass separator where the final ^{177}Lu extraction takes place. The second method implies that the facility makes use of samples irradiated in nuclear reactors or medical accelerators, as well as samples from nuclear waste depositories.

This paper is a review of the work carried out at the National Research Center Kurchatov Institute in order to study the capabilities of selective laser photoionization to obtain ^{177}Lu as a medical pharmaceutical. The research addressed not only the purely scientific aspects of isotope extraction, which are of independent importance for atomic spectroscopy, such as the search for an effective optical photoionization scheme and its kinetic parameters and the study of the hyperfine structure of the scheme and isotopic shifts, but also applied aspects of isotope separation: isotopic selectivity, degree of extraction, etc.

2. Experimental facility and measuring techniques

The studies were carried out by the method of Laser Resonance Ionization Mass Spectrometry (LRIMS) [18, 19] on a setup designed for spectroscopic experiments with narrow collimated atomic beams with the possibility of determining the isotopic composition of photoions produced during laser-induced photoionization. The setup consists of a vacuum chamber with an evacuation system and a tantalum evaporator placed inside the chamber of a quadrupole mass spectrometer. A commercial MS-7302 quadrupole mass spectrometer was used. The resolving power of the mass spectrometer was ~ 200 and, when tuned to a certain isotope, the contribution to the signal amplitude from neighboring isotopes did not exceed 10^{-4} of the amplitude of the latter.

Due to a system of apertures, lutetium atoms formed an atomic beam with a total opening angle of 3°. The atomic beam was crossed by the laser beam directly in the ionization chamber of the ion source of the mass spectrometer (Fig. 1). The directions of the atomic beam, laser radiation, and the ion-optical axis of the mass spectrometer were mutually perpendicular. The Doppler broadening of the lines under

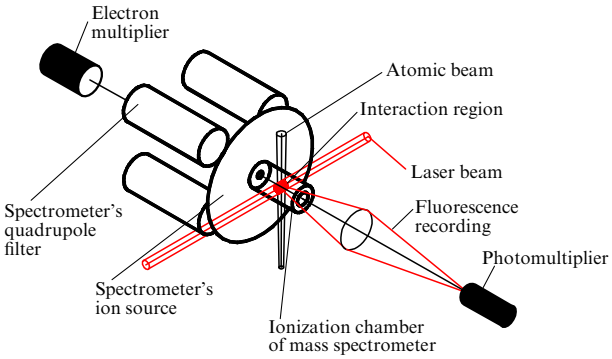

Figure 1. Schematic diagram for recording photoion current and fluorescence.

these conditions was ~ 100 MHz. In the chamber, the laser beam passed through an aperture stop, which was placed directly in front of the evaporation zone and selected the most uniform central part of the beam. The zone of interaction between light and vapor was a cylinder 2 mm long and 2 mm in diameter. Photoions were detected in the mass spectrometer using a secondary electron multiplier, and fluorescence was recorded using a photomultiplier located on the ion-optical axis of the spectrometer in the direction opposite to the photoion flow.

Metallic lutetium of a natural isotopic composition was used in the experiments. To conduct studies with the ^{177}Lu radioisotope and the ^{177m}Lu isomer, the samples were exposed to a neutron flux of $(1.5-3) \times 10^{13}$ cm^{-2} s^{-1} of the IR-8 reactor for 1 and 49 days, respectively.

The laser system comprised pulsed dye lasers (DLs) with lasing in the visible range pumped by copper vapor lasers (CVLs). The DL system had three independent channels, each of which consisted of a master oscillator (MO) and an amplifier. The master oscillators operated by a single longitudinal mode and were built according to the Littman framework with a grazing incidence diffraction grating [20]. Two DL channels (laser dye: Pyrromethene-556 in ethanol; lasing range: 532–555 nm) were pumped with the green component of the CVL (510 nm), and one DL channel (Sulforhodamine-640 in ethanol: 605–620 nm) was pumped with the yellow component of the CVL (578 nm). The output power level of single-mode MO oscillation was 100–200 mW; the spectral width of the laser line was 100–150 MHz (FWHM, full width at half maximum), the frequency-nonselective background did not exceed 0.6%, the pulse duration was 15–20 ns (FWHM), and the pulse repetition rate was 10 kHz. The average output power of the MO was raised to a level of several watts in DL amplifiers. All MOs had the capacity to scan the laser wavelength by changing the voltage on the piezodrive of the resonator's rotary mirror. The radiation wavelength of each DL was monitored using LM007 precision λ-meters (Laser 2000, GmbH), which provided an absolute accuracy of wavelength measurements of ~ 0.0005 Å. If necessary, λ-meters were used as a stabilized reference for transferring any DL to the mode of active wavelength stabilization. The output DL frequency was stabilized automatically by controlling the length of the MO resonator using a piezodrive of the input resonator mirror. The deviation of the laser line center from the preset value in the long-term stabilization mode did not exceed ± 40 MHz. More detailed information about the DL system can be found in Ref. [21].

The DL beams at the output of the amplifiers were telescoped to a size of $\varnothing = 12$ mm. Their spatial convergence into a single beam was carried out using semitransparent and dichroic mirrors. The three-color radiation was next directed to the mass spectrometric chamber. Control of the laser system, data recording, and their preliminary processing were carried out online [22].

3. Photoionization scheme

The ionization threshold of a lutetium atom is 43,762.60 cm^{-1}. For radiation in the visible range, this means that three quanta are needed to overcome this threshold, i.e., the excitation scheme should be three-stage. The electronic configuration of the ground state of the LuI atom is $4f^{14}5d6s^2\ ^2D_{3/2}$. Since the 4f shell is completely filled, its electrons hardly participate in electronic transitions between levels, and the spectrum of optical transitions in lutetium is not as rich as in most other rare earth elements. Detailed information on atomic levels and spectral lines of optical transitions is contained in Refs [23–25]. For a CVL-pumped DL system, the choice of the first and second excitation levels was virtually the only option. The strongest transitions are those with wavelengths of 5404 Å (first stage) and 5350 Å (second stage) to the states $5d6s6p\ ^4F^0_{5/2}$ and $5d6s7s\ ^4D_{3/2}$, respectively, and so the task was to find an effective autoionizing state (AIS).

The search for the transition to the AIS from the $5d6s7s\ ^4D_{3/2}$ level was performed using three DLs, two of which were tuned to resonance with the first and second transitions (DL1 and DL2, respectively). The DL of the third stage (DL3) was scanned in the spectral range of dye tuning with simultaneous recording of the photoion signal. When a peak was detected, a check was made for the relation between the resonance and the second transition. If the photoion signal disappeared when DL2 was completely intercepted, then the detected resonance was recorded as an autoionization (AI) transition. The search for AIS was carried out in two spectral ranges: 5640–5907 Å (Pyrromethene-597 dye) and 6050–6300 Å (Sulforhodamine-640, Cresyl Violet). The data are collected in Table 1. The autoionization transition with an in-air wavelength of 6178.77 Å to a state with an energy of 53,375 cm^{-1} turned out to be the brightest one [12]. Therefore, the optical scheme of LuI photoionization, which was used in further studies, is as follows:

$$5d6s^2\ ^2D_{3/2}\ (0\ \text{cm}^{-1}) \rightarrow 5d6s6p\ ^4F^0_{5/2}(18{,}504.58\ \text{cm}^{-1}) \rightarrow 5d6s7s\ ^4D_{3/2}(37{,}193.98\ \text{cm}^{-1}) \rightarrow (53{,}375\ \text{cm}^{-1})^0_{1/2}$$

(Fig. 2). Note that Indian authors have recently published a number of papers on the photoionization of the isotopes ^{176}Lu and ^{176}Yb. New optical excitation schemes were proposed and calculations based on the density matrix formalism were performed in a quest for optimal photoionization conditions [26–28]. The search for odd autoionization states of LuI in the range of 50,650–51,650 cm^{-1} was also the concern of recent Ref. [29].

Since the ^{175}Lu, ^{176}Lu, ^{177}Lu, and ^{177m}Lu isotopes have a nonzero nuclear spin, all energy levels are split into multiplets (see Fig. 2). The sublevels in the multiplet are determined by the total atomic momentum $F = J + I, J + I - 1, \ldots, |J - I|$, where J is the total electron momentum of the atom, and I is

Table 1. AI transitions observed in the spectral ranges* 5640–5907 Å and 6050–6300 Å.

Wavelength (in air), Å	Photoion signal, arb. units	Wavelength (in air), Å	Photoion signal, arb. units
5640.37	30	5793.88	3
5646.27	18	5799.99	5
5661.17	15	5802.00	6
5724.50	23	5866.83	6
5737.44	350	5884.70	10
5770.79	18	5901.17	15
5777.49	35	6128.60	60
5786.03	30	6145.77	70
5787.10	35	6156.25	80
5793.88	3	6178.77	500

* Arbitrary units of the magnitudes of photoionization signals in different ranges do not coincide.

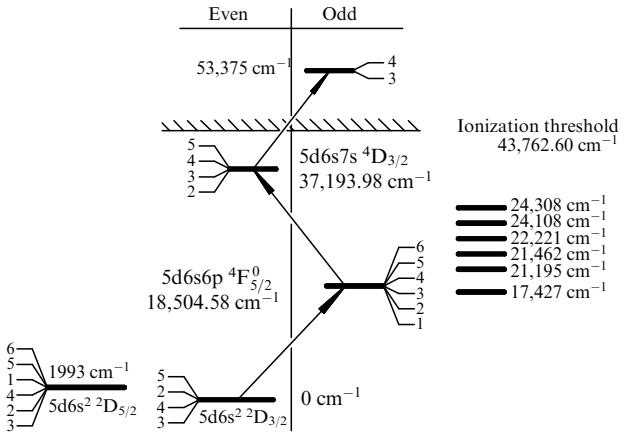

Figure 2. Photoionization scheme of ^{175}Lu and ^{177}Lu ($I = 7/2$) lutetium isotopes.

the nuclear spin. The hyperfine structure (HFS) spectrum arises from transitions between sublevels of multiplets with a change in the momentum $\Delta F = 0, \pm 1$; as a result, the optical photoionization spectrum for each isotope consists of 30 lines. The line frequency difference, as a rule, significantly exceeds the spectral lasing widths. Therefore, at a certain setting of the lasers, photoionization proceeds only along one chain of lines of the first, second, and third stages: the photoionization channel. The number of possible channels, taking into account the selection rules, amounts to 44. Obviously, the search for selective channels for the extraction of the target isotope (along the lines with the greatest frequency separation from background isotopes) is possible only proceeding from a detailed study of the hyperfine structure of transitions at all stages of the photoionization scheme for each isotope.

Hyperfine splitting (energy shift $\Delta\nu_F$ of sublevels relative to the 'center of gravity' of the multiplet) is described using the constants of the magnetic dipole, A, and electric quadrupole, B, interactions and depends on I, J, and F [30]:

$$\Delta\nu_F = \frac{A}{2}\,K + \frac{B}{4}\,\frac{(3/2)K(K+1) - 2I(I+1)\,J(J+1)}{IJ(2I-1)(2J-1)}\,, \quad (1)$$

where

$$K = F(F+1) - J(J+1) - I(I+1)\,. \quad (2)$$

For each hyperfine structure line, one can write

$$E_{\rm e} - E_{\rm g} + \Delta\nu_{F'} - \Delta\nu_F = \frac{1}{\lambda_{FF'}}\,, \quad (3)$$

where $E_{\rm e}$, $E_{\rm g}$ is the energy of the centers of gravity of the upper, e, and lower, g, multiplets (levels) of the transition, and $\lambda_{FF'}$ [cm^{-1}] is the wavelength of the $F \to F'$ line.

The energy E of the center of gravity of the level is determined from the condition

$$\sum_F (E_F - E)(2F+1) = 0\,, \quad (4)$$

where E_F is the energy of the sublevel with momentum F.

The energy difference between the centers of gravity for different isotopes determines the isotopic level shift.

Results of the first experiments to determine the HFS scheme,

$$5d6s^2\ ^2D_{3/2}\ (0\ \text{cm}^{-1}) \to 5d6s6p\ ^4F^0_{5/2}(18{,}504.58\ \text{cm}^{-1}) \to 5d6s7s\ ^4D_{3/2}(37{,}193.98\ \text{cm}^{-1}) \to (53{,}375\ \text{cm}^{-1})^0_{1/2}\,,$$

for natural isotopes were obtained in Ref. [12]. In Ref. [13], the hyperfine structure of the 5d6s^2 ^{2}D$_{3/2}$ $\to$ 5d6s6p ^{4}F$^0_{5/2}$ transition for the ^{177}Lu radioisotope was studied for the first time. The results of the HFS study at all stages for the ^{175}Lu, ^{176}Lu, and ^{177}Lu isotopes are presented in Ref. [31], and for the ^{177m}Lu isomer, in Ref. [32].

The wavelengths of all 12 ^{175}Lu HFS lines of the first stage 5d6s^2 ^{2}D$_{3/2}$ $\to$ 5d6s6p ^{4}F$^0_{5/2}$ were determined by fluorescence spectroscopy. When scanning the DL1 wavelength in the vicinity of the transition ($\sim$ 20 GHz), the fluorescence signal was recorded (from the first excited level 5d6s6p ^{4}F$^0_{5/2}$). At the same time, the wavelengths of 7 out of 12 ^{176}Lu lines were measured. Some of the lines were blended by the ^{175}Lu lines, mainly due to the difference in the natural abundance of the isotopes ($\sim$ 30 times) and, accordingly, in the fluorescence signals. The F-identifications of the lines and the determination of the remaining ^{176}Lu lines were performed proceeding from the splitting of the 5d6s^2 ^{2}D$_{3/2}$ and 5d6s6p ^{4}F$^0_{5/2}$ levels [33–35].

In view of the extremely low content of ^{177}Lu and ^{177m}Lu isotopes in a sample under evaporation ($\sim 10^{-5}$), their hyperfine structure was studied by resonance ionization mass spectroscopy. The wavelengths of the ^{177}Lu first stage lines were initially determined by calculation. Due to the equity of nuclear spins ($I = 7/2$) and close values of nuclear magnetic dipole moments ($\mu_{177} = 2.2384(14)\,\mu_{\rm N}$ [36], $\mu_{175} = 2.2323(11)\,\mu_{\rm N}$ [37]), the patterns of hyperfine splitting of ^{177}Lu and ^{175}Lu levels are similar. In this case, all ^{177}Lu lines are simply shifted by the isotopic shift relative to the corresponding ^{175}Lu lines. The isotopic shift at the transition of the first excitation stage $6s^2 \to 6s6p$ is determined by the field component (the mass component is small and does not exceed 20 MHz [38, 39]). The field shift is due to the difference in the root-mean-square charge radii $\delta\langle r^2\rangle$ of the corresponding isotopes. According to Ref. [35], the difference in the root-mean-square charge radii $\delta\langle r^2\rangle$ for the ^{177}Lu and ^{175}Lu isotopes is

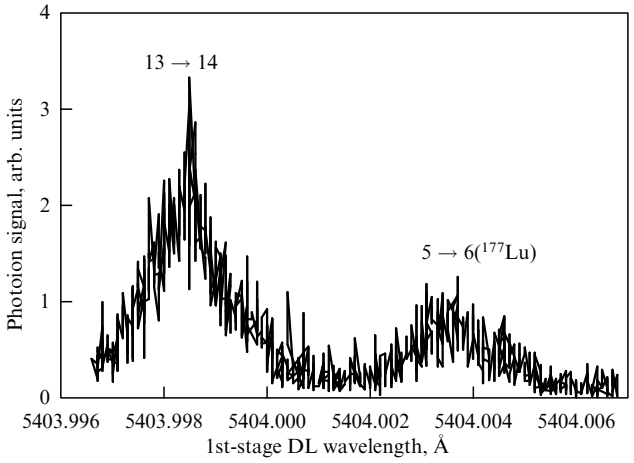

Figure 3. ^{177m}Lu and ^{177}Lu photoion signals in the scanning of the first-stage DL wavelength for DL2 ($14 \to 13$) = 5350.6445 Å and DL3 ($13 \to 12$) = 6180.1151 Å [32].

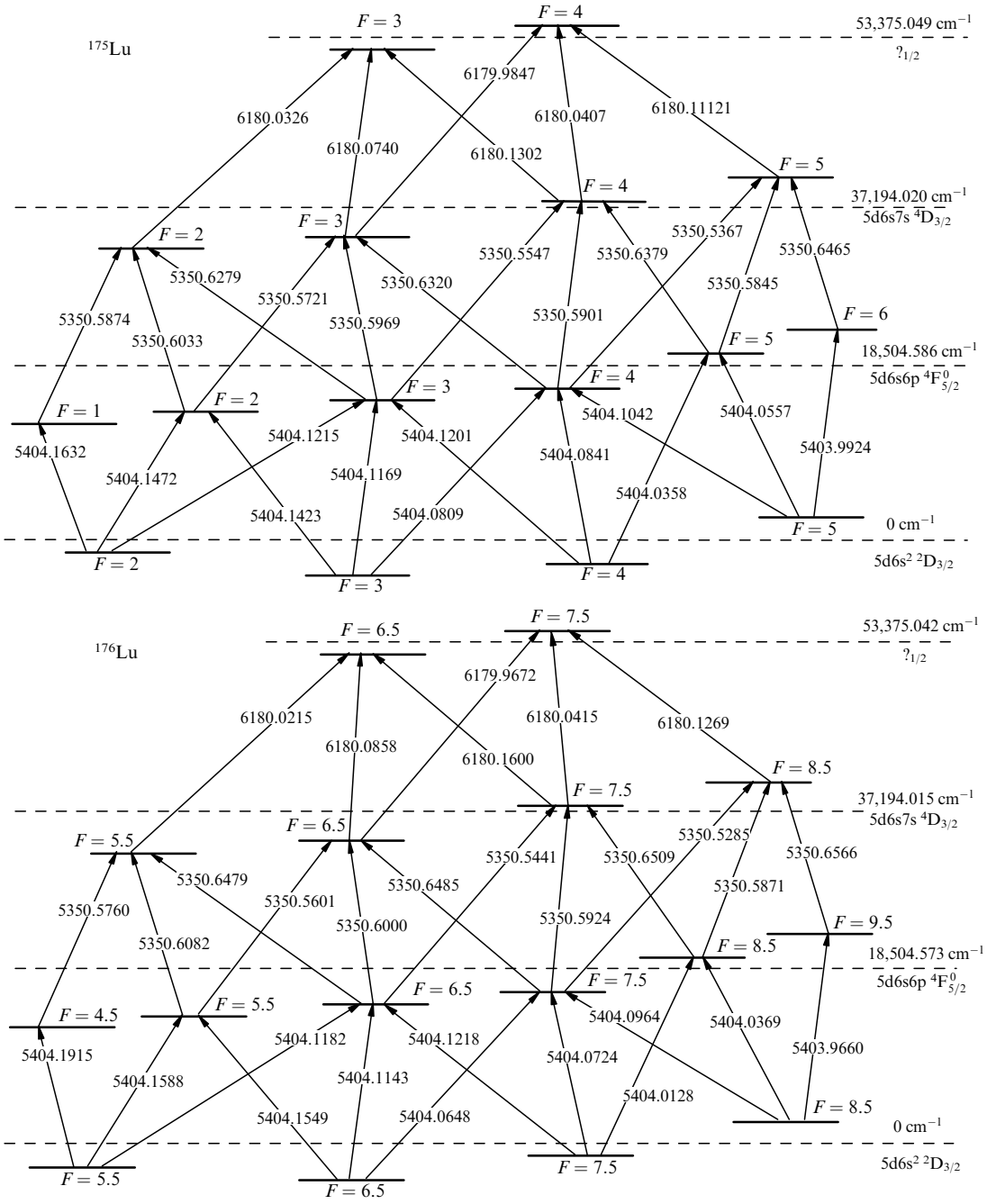

Figure 4. Photoionization schemes of ^{175}Lu ($I = 7/2$) and ^{176}Lu ($I = 7$) (vacuum wavelength units, Å) [31].

approximately three times greater than for ^{176}Lu and ^{175}Lu; hence, it follows that the isotopic shift of ^{177}Lu with respect to ^{175}Lu is also three times greater than the shift between ^{176}Lu and ^{175}Lu. The isotopic shift of the 5d6s6p $^4F^0_{5/2}$ level for ^{176}Lu is known: -388.8 MHz [40] and, accordingly, -1150 MHz for ^{177}Lu.

The wavelengths of the first stage lines for the ^{177m}Lu isomer were also initially predicted. The calculation used the fact that the ratios of the constants A and B of the upper and lower transition levels are the same for all isotopes within the hyperfine magnetic anomaly [41] and for the lower level $A_{177m}(5d6s^2\,{}^2D_{3/2}) = 61.2(3)$ MHz and $B_{177m}(5d6s^2\,{}^2D_{3/2}) = 2472(11)$ MHz [35]. An estimate of the isotopic shift, which was made by analogy with that in the case of ^{177}Lu, was -815 MHz. As a result, it turned out that for ^{177m}Lu only one first-stage line $10 \rightarrow 9$ coincided, within 30 MHz, with the line $2 \rightarrow 2$ of the main isotope ^{177}Lu and could not be spectrally resolved.

A feature of the experiments with the ^{177m}Lu isomer was that, in contrast to isotopes with different atomic masses recorded separately using traditional resonant ionization mass spectroscopy, ^{177}Lu and ^{177m}Lu have almost the same atomic masses. The difference between their masses is ~ 0.97 MeV [1], while the difference between the masses of neighboring isotopes is approximately 1000 MeV (the mass of one nucleon). Such a difference cannot be resolved by quadrupole mass spectrometers; therefore, only lines whose frequencies differed from the HFS lines of the main ^{177}Lu isotope by more than the laser linewidth (100–150 MHz) could be recorded in the experiment. Figure 3 shows an

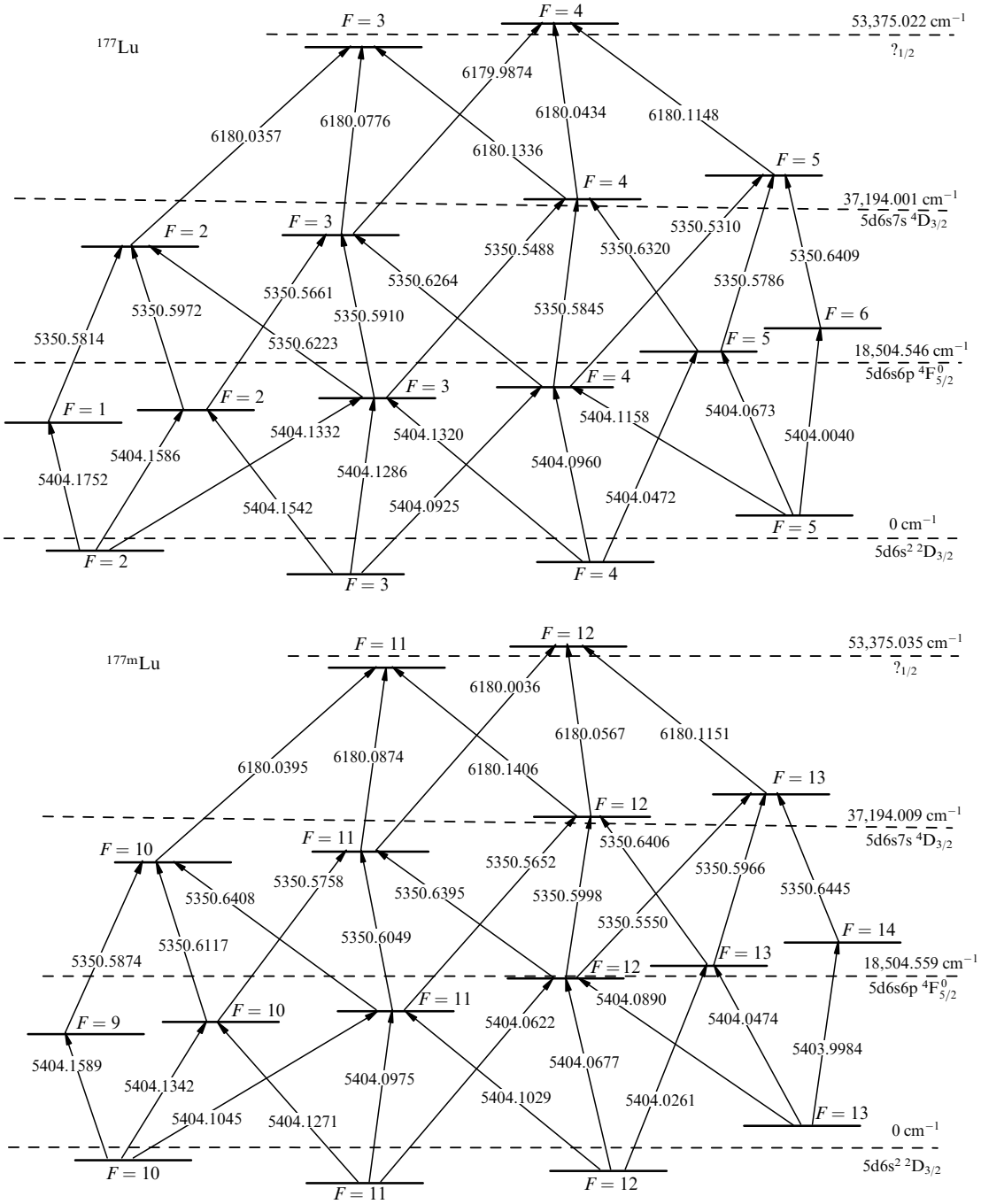

Figure 5. Photoionization schemes of ^{177}Lu ($I = 7/2$) and ^{177m}Lu ($I = 23/2$) (vacuum wavelength units, Å) [31, 32].

example of simultaneous selective detection of ^{177m}Lu and ^{177}Lu photoions.

When studying the HFS of the second transition 5d6s6p $^4F^0_{5/2} \rightarrow$ 5d6s7s $^4D_{3/2}$, the mass spectrometer was tuned to detect atomic mass 177, and DL1 was successively stabilized at the calculated wavelengths of each of the $F \rightarrow F'$ lines of the first transition. DL2 was scanned in the vicinity of 5305 Å and, at resonance with the transition, transferred atoms to the 5d6s7s $^4D_{3/2}$ level, and DL3 ionized the atoms into a continuum. During each scan, from one to three photoionization peaks were recorded (transitions with $\Delta F = 0, \pm 1$). Peaks corresponding to transitions to common upper sublevels F were determined from the equity of excitation photon energies, taking into account the hyperfine splitting of the ground level 5d6s^2 $^2D_{3/2}$ [35]. The number of such peaks and their location in the spectra made it possible to identify the quantum numbers F of the lower and upper sublevels for all lines of the second transition for isotopes ^{175}Lu, ^{176}Lu and ^{177}Lu, ^{177m}Lu (12 lines each).

During the study of the HFS of the third transition 5d6s7s $^4D_{3/2} \rightarrow (53{,}375\ \text{cm}^{-1})^0_{1/2}$, DL1 and DL2 were stabilized at the lines determined at the previous stages of the experiment. DL3 was scanned near the 6180 Å AI transition. All lines of the third transition (six lines) were spectrally resolved and identified in F. After that, the values of the wavelengths of the first stage were refined. DL2 and DL3 were stabilized at known wavelengths, and DL1 was scanned near the calculated resonances.

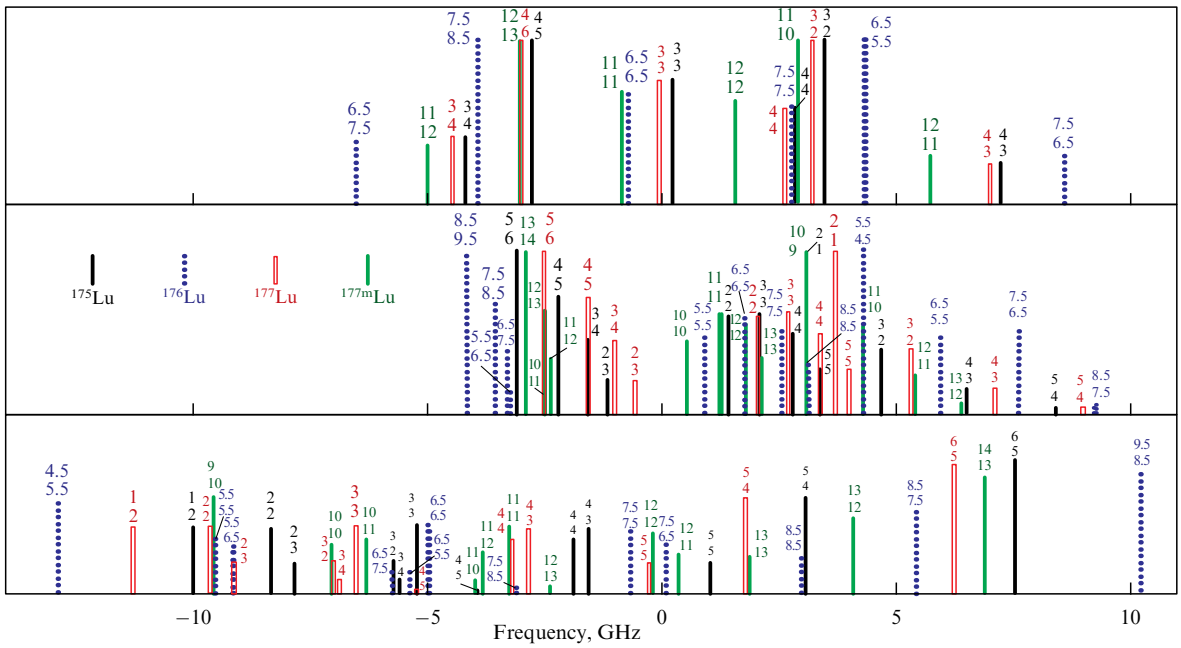

Figure 6. Hyperfine structure of photoionization transition scheme $5d6s^2\ ^2D_{3/2}(0\,cm^{-1}) \rightarrow 5d6s6p\ ^4F^0_{5/2}(18{,}504.58\ cm^{-1}) \rightarrow 5d6s7s\ ^4D_{3/2}$ $(37{,}193.98\ cm^{-1}) \rightarrow (53{,}375\ cm^{-1})^0_{1/2}$ of the isotopes ^{175}Lu, ^{176}Lu, ^{177}Lu, and ^{177m}Lu. Bottom row — lines of the 1st transition, in middle row — 2nd transition, top row — 3rd transition; relative height of the lines is proportional to the transition cross section.

In order to avoid the influence of two-photon processes on the accuracy of measurements in the study of the HFS of the first stage, the DL2 and DL3 pulses were delayed relative to the DL1 pulse by the pulse duration (20 ns). In the study of the HFS of the second and third stages, all pulses were separated in time. To determine the center of each line (the exact value of the wavelength $\lambda_{FF'}$), the experimental points of photoionization resonances were approximated by the Voigt profile using the least squares method.

The results of experiments in the form of photoionization schemes for ^{175}Lu, ^{176}Lu, ^{177}Lu, and ^{177m}Lu isotopes are shown in Figs 4 and 5. In Figure 6, all lines are brought together on a common frequency scale for each stage of the scheme.

The system of linear equations (3) for all recorded $\lambda_{FF'}$ lines was solved with respect to the constants A and B of the upper and lower levels and $(E_e - E_g)$ by means of χ^2-optimization for each stage of the scheme (number of $\lambda_{FF'}$ usually exceeded the number of unknowns in the equation). The results are summarized in Table. 2.

As is obvious from the diagram in Fig. 6, for the ^{177}Lu and ^{177m}Lu isotopes, there are excitation lines with a significant ($\sim$ 1 GHz) distance from the lines of natural isotopes, which can be used for their selective extraction from a mixture of isotopes of irradiated natural lutetium.

4. Level lifetimes

The efficiency of photoionization, as well as the choice of appropriate laser radiation intensities, largely depends on the decay characteristics of the excited states. If the level lifetime turns out to be comparable to or shorter than the laser pulse duration, then a significant part of the particles spontaneously leave the excited level. In this case, it turns out to be critically important whether the decay occurs back to the previous state, or whether the particle passes into another, third-party state that does not participate in the photoionization scheme. In the former case, the particle can be re-excited by laser radiation and can further contribute to the separation product, in which case the particle is lost and the degree of extraction of the target isotope decreases. In the scheme under consideration, the lifetime of the first excited state $5d6s6p\ ^4F^0_{5/2}$ is known (472 ns), and the decay occurs into the ground state $5d6s^2\ ^2D_{3/2}(0)$ and the metastable state $5d6s^2\ ^2D_{5/2}$ ($1993\ cm^{-1}$) with branching ratios of 0.566 and 0.434, respectively [42].

There is no information on the lifetime of the second excited state $5d6s7s\ ^4D_{3/2}$ in the literature. The lifetime of the $5d6s7s\ ^4D_{3/2}$ level determined experimentally (Fig. 7) is 11.5 ns [31]. Spontaneous decay from the $5d6s7s\ ^4D_{3/2}$ level occurs, in addition to $5d6s6p\ ^4F^0_{5/2}$, into six other levels (Table 3) [25]. Atoms that have passed to these levels are lost for the photoionization process, since the DL photon energy

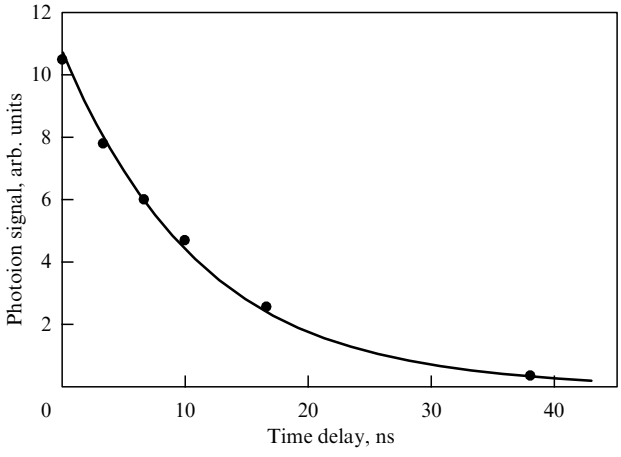

Figure 7. Dependence of the ^{175}Lu photoion signal in the ionization channel $2 \rightarrow 1 \rightarrow 2 \rightarrow 3$ on the time delay of the third-stage DL relative to DL1 and DL2 and approximating curve $y = 10.8 \exp(-x/11.5)$ [31].

Table 2. Energy, isotopic shifts relative to ^{175}Lu, and hyperfine splitting constants for levels of the photoionization scheme for ^{175}Lu, ^{176}Lu, ^{177}Lu, and ^{177m}Lu.

Level	Isotope (nuclear spin)	Energy, cm^{-1}	A, MHz	B, MHz	Isotopic shift, MHz	References
5d6s^2 ^{2}D$_{3/2}$	175(7/2)	0	194.4(7)	1509(6)	0	[35]
	176(7)	0	137.6(5)	2132(11)	0	[35]
	177(7/2)	0	194.9(6)	1467(5)	0	[35]
	177m(23/2)	0	61.2(3) 61.2(8)	2472(11) 2466(40)	0	[35] [32]
5d6s6p ^{4}F$^0_{5/2}$	175	18,504.5864(21)	987.5(2,2) 987.35(12)	1103(43) 1117.9(2.0)	0	[31] [50]
	176	18,504.5733(19)	697.8(0.8) 698.25(15)	1566(29) 1572.2(3.0)	−390(14) −388.8(11)	[31] [50, 40]
	177	18,504.5463(22)	988.8(2.8)	1059(55)	−1201(20)	[31]
	177m	18,504.5593(20)	310.5(8)	1840(63)	−812(25)	[32]
5d6s7s ^{4}D$_{3/2}$	175	37,194.0202(26)	1105.2(2.8)	74(33)	0	[31]
	176	37,194.0149(22)	781.0(1.3)	78(30)	−160(30)	[31]
	177	37,194.0007(27)	1107.6(5.8)	48(46)	−605(46)	[31]
	177m	37,194.0082(27)	348(2)	134(68)	−360(57)	[32]
(53,375 cm^{-1})$^0_{1/2}$	175	53,375.0494(35)	1752(18)	0	0	[31]
	176	53,375.0421(27)	1240.5(5.6)	0	−201(55)	[31]
	177	53,375.0217(41)	1764(22)	0	−822(81)	[31]
	177m	53,375.0324(43)	549(6)	0	−507(120)	[32]

Table 3. Einstein coefficients A_{eg} for transitions from levels 18,504.580 cm^{-1} and 37,193.980 cm^{-1} [25].

Transition wavelength (in the air), Å	Energy of lower level g, cm^{-1}	Energy of upper level e, cm^{-1}	Einstein coefficient A_{eg}, 10^6 s^{-1}
5402.566	0	18,504.580	1.176
6055.017	1993.920	18,504.580	1.126
5057.603	17,427.280	37,193.980	21.57
5349.139	18,504.580	37,193.980	32.01
6248.814	21,195.370	37,193.980	7.417
6354.875	21,462.380	37,193.980	8.622
6677.157	22,221.680	37,193.980	1.709
7640.084	24,108.720	37,193.980	7.864
7758.291	24,308.090	37,193.980	7.985

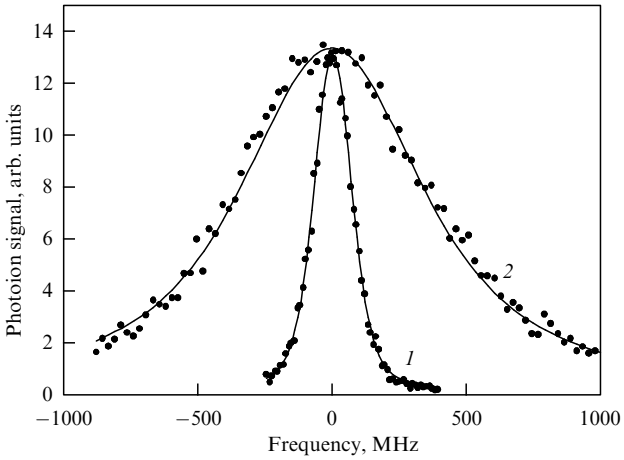

Figure 8. ^{176}Lu photoion signal (experimental points) during scanning: DL2 near (*1*) transition 5d6s6p ^{4}F$^0_{5/2}$ → 5d6s7s ^{4}D$_{3/2}$ (4.5 → 5.5; 5350.5760 Å) and DL3 near (*2*) transition 5d6s7s ^{4}D$_{3/2}$ → AIS (53,375 cm^{-1})$^0_{1/2}$ (5.5 → 6.5; 6180.0215 Å). Solid curves are Voigt profiles with widths $\Delta\nu_{9/2\text{–}11/2}$ (FWHM) = 150 MHz and $\Delta\nu_{11/2\text{–}13/2}$ (FWHM) = 900 MHz, respectively [31].

is high enough to excite them above the ionization threshold. According to Table 3, the branching ratios to the 5d6s6p ^{4}F$^0_{5/2}$ state and to the side levels are 0.367 and 0.633, respectively, and the lifetime of 5d6s7s ^{4}D$_{3/2}$ is 11.5 ns, which coincides with the experimental data.

The 900 MHz width of the observed photoionization resonance (Fig. 8) arises both from the width of the autoionization state itself and from the 150 MHz width of the second excited state, from which photoionization occurs. Therefore, the 750 MHz broadening of the line arising from the third transition 5d6s7s ^{4}D$_{3/2}$–AIS (53,375 cm^{-1})$^0_{1/2}$ is associated only with the width of the upper level and corresponds to its lifetime $\tau = 0.21(4)$ ns.

5. Transition cross sections

The photoionization scheme levels have a developed hyperfine structure (see Figs 4–6), which, together with selection rules, gives 44 different combinations of sublevels — channels through which photoionization can be performed. With a certain laser tuning, photoionization occurs in only one channel; the differences among the transition frequencies of different channels for each isotope, as a rule, significantly exceed the spectral laser widths. The channels differ in wavelengths and transition probabilities. The saturation of scheme transitions was investigated in Ref. [43] in order to determine the effective cross sections for excitation of various components of the hyperfine structure for the isotopes ^{175}Lu, ^{176}Lu, ^{177}Lu, and ^{177m}Lu.

Table 4. Angular coefficients $C(F, J, F', J', I)$ of cross sections [43].

$5d6s^2\,{}^2D_{3/2}$	1st transition	$5d6s6p\,{}^4F^0_{5/2}$	2nd transition	$5d6s7s\,{}^4D_{3/2}$	3rd transition	AIS ($53{,}375\ cm^{-1}$)
F	$C(F, J, F', J', I)$	F	$C(F, J, F', J', I)$	F	$C(F, J, F', J', I)$	F
^{175}Lu and ^{177}Lu ($I = 7/2$)						
2	0.4 0.4 0.2	1 2 3	1 0.6 0.214	2	1	3
3	0.19 0.417 0.393	2 3 4	0.4 0.625 0.458	3	0.75 0.25	3 4
4	0.083 0.33 0.587	3 4 5	0.161 0.495 0.72	4	0.417 0.583	3 4
5	0.025 0.187 0.788	4 5 6	0.047 0.28 1	5	1	4
^{176}Lu ($I = 7$)						
5.5	0.556 0.328 0.116	4.5 5.5 6.5	1 0.492 0.149	5.5	1	6.5
6.5	0.29 0.418 0.291	5.5 6.5 7.5	0.507 0.627 0.383	6.5	0.711 0.289	6.5 7.5
7.5	0.13 0.367 0.503	6.5 7.5 8.5	0.223 0.551 0.671	7.5	0.378 0.622	6.5 7.5
8.5	0.04 0.22 0.741	7.5 8.5 9.5	0.067 0.329 1	8.5	1	7.5
^{177m}Lu ($I = 23/2$)						
10	0.603 0.30 0.094	9 10 11	1 0.455 0.128	10	1	11
11	0.332 0.414 0.254	10 11 12	0.545 0.62 0.351	11	0.694 0.306	11 12
12	0.154 0.367 0.465	11 12 13	0.251 0.571 0.646	12	0.361 0.639	11 12
13	0.048 0.238 0.716	12 13 14	0.078 0.354 1	13	1	12

The partial cross section for the transition between the hyperfine component F of level 1 and the component F' of level 2 can be written as [44]

$$\sigma_{FF'} = C(F, J, F', J', I)\tilde{\sigma}_{12}\,, \tag{5}$$

where $\tilde{\sigma}_{12}$ is the total cross section of transition $1 \to 2$, and $C(F, J, F', J', I)$ is the angular coefficient depending on the angular momentum involved in the transition. The angular coefficients for ^{175}Lu, ^{176}Lu, ^{177}Lu, and ^{177m}Lu isotopes calculated using formulas from Ref. [44] are collected in Table 4.

Studied in our experiments was the dependence of the photoion current on the radiation intensity of the DL, which was successively tuned to each HFS line of a particular transition of the scheme (Fig. 9). The study of the lines of the first and second stages was performed with pulses separated in time. In this case, within each pulse, the atomic system can be considered a two-level one, and the intensity dependence can be obtained from the solution of the system of two kinetic equations

$$\frac{\mathrm{d}N_i}{\mathrm{d}t} = -N_i w_{ik} + N_k w_{ki}\,, \tag{6}$$

$$\frac{\mathrm{d}N_k}{\mathrm{d}t} = N_i w_{ik} - N_k(w_{ki} + a)\,. \tag{7}$$

Here, N_i and N_k are the numbers of particles in the lower and upper states, respectively, a is the frequency of decays from state k, w_{ik} is the frequency of laser-induced transitions from

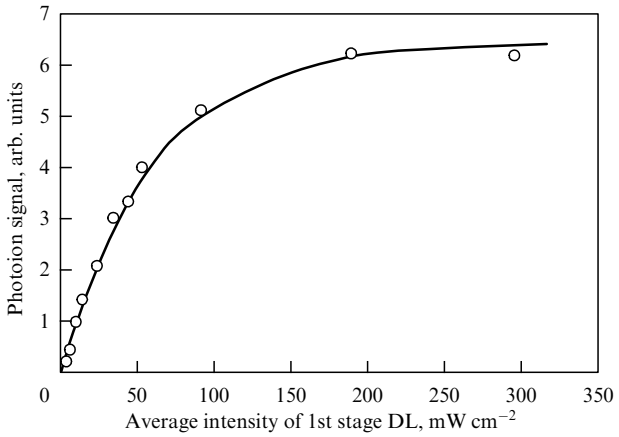

Figure 9. Dependence of the ^{176}Lu photoion current on the average output power of first-stage DL $8.5 \rightarrow 7.5$ (experimental points) and approximative curve (7) for the transition cross section $\sigma_{8.5\text{–}7.5} = 3.2 \times 10^{-14}$ cm^2 [43].

state i to state k, $w_{ik} = \bar{I}\sigma_{ik}/(h\nu_{ik})$, where $\bar{I}$ is the laser radiation intensity [W cm^{-2}], σ_{ik} is the transition cross section [cm^2], and ν is the transition frequency $i \rightarrow k$.

The solution of system (6), (7) under the condition of a rectangular laser pulse is of the form

$$N_k(\tau) = \frac{N_0 w_{ik}}{A}\left[\exp\left(\frac{-\bar{B}+\bar{A}}{2}\,\tau\right) - \exp\left(\frac{-\bar{B}-\bar{A}}{2}\,\tau\right)\right], \quad (8)$$

where

$$\bar{A} = \frac{g_i + g_k}{g_k}\,w_{ik} + a\,, \quad \bar{B} = \sqrt{\left(\frac{g_i + g_k}{g_k}\,w_{ik} + a\right)^2 - 4a\,w_{ik}}\,,$$

with g_i and g_k being the statistical weights of the states i and k, respectively.

The third transition was studied using pulses coincident in time, with deep saturation of the first and second transitions. Under these conditions, a bottleneck effect occurs at the third transition, and the number of photoions formed by the end of the pulse can be approximated by a function obtained in Ref. [45]:

$$N_i(\tau) = \frac{N_0 w_{34}}{w_{34} + a_{3M}}\left[1 - \exp\left(-\frac{g_3(w_{34} + a_{3M})}{g_1 + g_2 + g_3}\,\tau\right)\right], \quad (9)$$

where N_0 and N_i are the numbers of particles in the initial and final AI states, respectively; g_1, g_2, and g_3 are the statistical weights of the initial, first, and second excited states; a_{3M} is the decay rate from the second excited state; w_{34} is the frequency of laser-induced transitions from the second excited state to the AIS; $w_{34} = \bar{I}\sigma_{34}/(h\nu_{34})$, σ_{34} is the cross section of the third transition [cm^2]; and ν_{34} is the frequency of the third transition.

It is pertinent to note that some lines coincided to within 400 MHz with excitation lines from other lower sublevels [31]. With increasing intensity, the excitation and subsequent ionization of atoms from these sublevels had a noticeable effect on the dependence of the photoion current on the laser radiation intensity and made it impossible to determine the individual cross sections for these transitions. These lines include pairs $2 \rightarrow 3$, $4 \rightarrow 3$ and $3 \rightarrow 4$, $4 \rightarrow 4$ for isotopes ^{175}Lu and ^{177}Lu, $5.5 \rightarrow 6.5$, $7.5 \rightarrow 6.5$ and $5.5 \rightarrow 5.5$, $6.5 \rightarrow 5.5$ for ^{176}Lu, and $10 \rightarrow 11$, $12 \rightarrow 11$ and $11 \rightarrow 12$, $12 \rightarrow 12$ for ^{177m}Lu. The total effective cross sections for each transition were extracted by formula (5) from the condition of minimizing the sum of squared deviations from the experimental measurement data of the cross sections of the HFS transition components. The results for ^{175}Lu, ^{177}Lu, ^{176}Lu, and ^{177m}Lu are collected in Table 5. The cross sections for ^{177}Lu did not differ from the corresponding values for ^{175}Lu within the experimental errors.

Table 5. Total effective cross sections of the $5d6s^2\,{}^2D_{3/2} \rightarrow 5d6s6p\,{}^4F^0_{5/2} \rightarrow 5d6s7s\,{}^4D_{3/2} \rightarrow (53{,}375\ \text{cm}^{-1})^0_{1/2}$ transitions of the photoionization scheme [43].

Isotope	$\tilde{\sigma}_{01}$, cm^2	$\tilde{\sigma}_{12}$, cm^2	$\tilde{\sigma}_{23}$, cm^2
^{175}Lu, ^{177}Lu	$4.5(1) \times 10^{-13}$	$1.6(3) \times 10^{-12}$	$1.2(2) \times 10^{-14}$
^{176}Lu	$5(1) \times 10^{-13}$	$3.5(5) \times 10^{-12}$	$1.5(3) \times 10^{-14}$
^{177m}Lu	$5(1) \times 10^{-13}$	$2.3(3) \times 10^{-12}$	$2.1(3) \times 10^{-14}$

6. Degree of target isotope extraction in photoionization

One of the most important parameters of any isotope separation procedure is the fraction of atoms of the target isotope that enters the product, i.e., the degree of extraction of the target isotope from the feed stream. For the laser photoionization method, the degree of extraction is the sum of the probability that vaporized atoms find their way into the laser-irradiated zone, the probability of irradiating a continuous stream of atoms with pulsed laser radiation, the probability of photoionization of the irradiated atom, and, finally, the probability of extracting a photoion to the product collector. All of the above factors depend on the specific configuration of the separation cell, except for the probability of photoionization of irradiated atoms, which depends on the properties of transitions in the photoionization scheme and the selected laser radiation intensities at each stage. With an increase in intensity, the degree of extraction increases almost linearly at low intensities; with a further increase, the growth slows down and saturation sets in. The physical reason for saturation is the depletion of atoms in the ground state. In this case, we can assume that all atoms that were at the initial level are converted into photoions. For example, when the ^{177}Lu radioisotope is photoionized from the sublevel $F = 5$ of the hyperfine structure ($F = 2, 3, 4, 5$) of the ground state $5d6s^2\,{}^2D_{3/2}$, the degree of extraction may be as high as $0.34 \times 0.72 = 0.24$, where the factor 0.72 is the population of the ground state at a lutetium evaporation temperature of 1700 °C, and 0.34 is the fraction of atoms that are at the sublevel with $F = 5$.

To confirm the possibility of achieving a given extraction degree, the method of direct measurement [46] (Fig. 10) was used, the idea of which was to minimize the influence of geometric factors and make the irradiation probability of evaporated atoms close to unity. A thin beam of atoms from the evaporator passed through an extended (8 cm) irradiation region. The region was formed as a result of repeated passage of the laser aigrette (radiation with three wavelengths), which made the irradiation probability of atoms, taking into account the Maxwellian distribution of atomic velocities, equal to 97%. The irradiation zone was located between metal plates with a potential difference of several hundred volts. This ensured almost 100% removal of photoions from the vapor flow, which was subsequently limited and hit the quartz sensor for measuring the deposition thickness. The fraction of atoms extracted from the flow due to photoioniza-

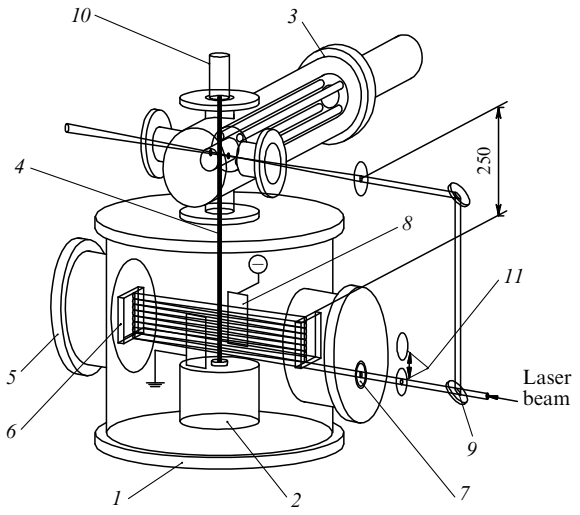

Figure 10. Facility for direct measurement of extraction degree: *1* — vacuum chamber, *2* — thermal evaporator, *3* — quadrupole mass spectrometer, *4* — atomic beam, *5* — flange of multipass system, *6* — multi-pass system mirror, *7* — window for input of laser radiation, *8* — extraction system, *9* — semitransparent mirror, *10* — quartz deposition sensor, *11* — beam shutter [45].

Table 6. Measurement data for ^{175}Lu extraction degree in channel $5 \to 6 \to 5 \to 4$ [45].

Average DL intensity, W cm^{-2}			Ground state depopulation degree	Extraction degree
1st stage	2nd stage	3rd stage		
0.025	0.025	2.5	0.88 ± 0.05	0.17 ± 0.03

Table 7. Measurement data of extraction degree using different HFS transition components [45].

Photoionization channel	Fraction of atoms on the lower sublevel F	Relative population of the lower sublevel F	Relative extraction degree
$5 \to 6 \to 5 \to 4$	0.34	1	1
$4 \to 4 \to 5 \to 4$	0.28	0.82	0.75 ± 0.1
$3 \to 4 \to 5 \to 4$	0.22	0.64	0.6 ± 0.1
$2 \to 1 \to 2 \to 3$	0.16	0.46	0.5 ± 0.1

tion was determined by comparing the film growth rates on the sensor under open and closed laser radiation. The presence of a mass spectrometer above the working volume when splitting off a small part of the laser radiation made it possible to measure the fraction of atoms remaining in the ground state and thereby estimate the degree of initial state depopulation.

The measurement data of the degree of extraction and depletion of the ground state in channel $5 \to 6 \to 5 \to 4$ of ^{175}Lu photoionization are collected in Table 6. The degree of extraction directly depends on the population of the initial state (the starting sublevel), which is confirmed experimentally (Table 7). The highest extraction of 17% was achieved in channel $5 \to 6 \to 5 \to 4$. Judging by the temperature population of the ground state and the fraction of atoms at the sublevel with $F = 5$, the probability of photoionization of the irradiated atom was 70%. This value turned out to be noticeably lower than the measured degree of depletion of

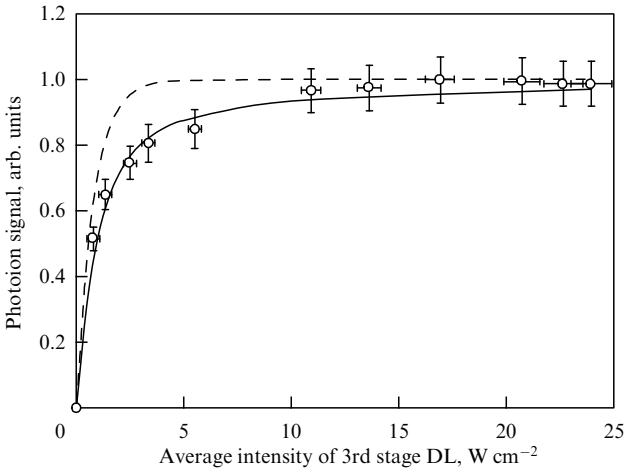

Figure 11. Dependence of the photoion signal on the average intensity of the third-stage DL (experimental points) in channel $5 \to 6 \to 5 \to 4$. Solid curve: calculation by formula (8) with a cross section $\sigma_{34} = 1.2 \times 10^{-14}$ cm^2 and a decay frequency $a_{3M} = 87$ MHz; dashed curve: $\sigma_{34} = 1.2 \times 10^{-14}$ cm^2 without decay, $a_{3M} = 0$ [45].

the initial state of 88%. The reason for this probably lies with the intense decay from the second excited state, whose lifetime is rather short, 11.5 ns [31].

Formula (9) was obtained in Ref. [45] to estimate the effect of decay on the probability of photoionization of an irradiated atom. The factor $w_{34}/(w_{34} + a_{3M})$ describes the competition between photoionization and spontaneous decay of the second excited state. This factor relatively quickly (when $w_{34} = a_{3M}$) reaches the value of 0.5, but its further increase slows down with increasing w_{34}, and even at $w_{34} = 5a_{3M}$ it is only 0.83. Achieving a photoionization degree above 0.9 requires so significant an increase in w_{34} that it seems to be beyond rationality. The effect of decay is well illustrated in Fig. 11, which shows the experimental dependence of the photoion signal on the DL3 intensity measured in a wide power range. One can see that saturation occurs at an average intensity of about 2.5 W cm^{-2} in the absence of decay (dashed curve). In the presence of decay (experimental points), the signal continues to increase at values of average intensity up to 17 W cm^{-2}, and, at 2.5 W cm^{-2}, the signal is ~ 0.7 of the saturation value.

With the simultaneous action of laser pulses of the first and second stages, photoionization is significantly affected by multiphoton processes, which lead to a decrease in selectivity. To increase the selectivity, one can use the delay of the DL2 and DL3 pulses with respect to the first stage pulse, taking into account the fact that the lifetime of the first excited state is rather long, 472 ns. In this case, however, a decrease in the extraction degree is inevitable, since not all atoms that were at the initial sublevel $F = 5$ become available for photoionization, but only those that populated the first excited state $F = 6$ after the end of the first stage pulse. In the case of saturation, the fraction of such atoms is $g_2/(g_1 + g_2) = 0.54$, where g_1 and g_2 are the statistical weights of the ground and first excited states, respectively. Direct measurement showed that, with a DL2 and DL3 delay of 20 ns, the degree of extraction was 0.6 ± 0.1 of that measured in the case of combined pulses, which is in good agreement with the above estimate.

Table 8. Selective ^{177}Lu photoionization channels (in terms of HFS components)* [31, 32].

^{177}Lu photoionization channel	Ionization channel Line shifts in stages relative to ^{177}Lu, MHz		
	^{175}Lu	^{176}Lu	^{177m}Lu
$5 \to 6 \to 5 \to 4$	$5 \to 6 \to 5 \to 4$ 1192; −587; 212	$7.5 \to -8.5 \to 7.5 \to 6.5$ −904; −1050; −3550	$13 \to 14 \to 13 \to 12$ +575; −377; −24
$5 \to 5 \to 5 \to 4$	$5 \to 5 \to 5 \to 4$ 1192; −618; 212	$6.5 \to 7.5 \to 7.5 \to 6.5$ 257; −1446; −3550	$12 \to 12 \to 13 \to 12$ −40; +2389; −24
$4 \to 3 \to 4 \to 3$	$4 \to 3 \to 4 \to 3$ 1222; −618; 267	$7.5 \to 6.5 \to 7.5 \to 6.5$ 1048; 493; −2074	$10 \to 10 \to 11 \to 11$ −226; −2829; +3629
$2 \to 3 \to 4 \to 3$	$2 \to 3 \to 4 \to 3$ 1202; −618; 267	$7.5 \to 6.5 \to 7.5 \to 6.5$ 1171; 493; −2074	$10 \to 10 \to 11 \to 11$ −100; −2829; +3629
$2 \to 1 \to 2 \to 3$	$2 \to 1 \to 2 \to 3$ 1233; −629; 244	$5.5 \to 5.5 \to 6.5 \to 6.5$ 1685; 2232; −3935	$10 \to 9 \to 10 \to 11$ +1674; −629; −298

* Indicated for each scheme are nearest ^{175}Lu, ^{176}Lu, and ^{177m}Lu isotope excitation channels and frequency distances to ^{177}Lu for all ionization stages.

7. Photoionization selectivity

In laser isotope separation, the selectivity achieved at the photoionization stage, along with the extraction degree, is the most important parameter of the separation.

Selectivity, defined as the ratio of the photoionization probabilities of the target isotope W_t and the nontarget isotope W,

$$S = \frac{W_t}{W}\,, \tag{10}$$

primarily depends on the magnitude of the spectral contrast, i.e., the fraction of laser radiation entering the absorption profile of a nontarget isotope, as well as on the ratio between the spectral width of laser radiation and the frequency difference between the absorption lines of the target and nontarget isotopes. For an initial content of the target isotope C_f, the number of photoions of the target isotope will be $W_t C_f$, the amount of the nontarget isotope will be $W(1 - C_f)$, respectively, and the concentration of C_p, the target isotope, in the ensemble of photoions will be

$$C_p = \frac{W_t C_f}{W(1 - C_f) + W_t C_f}\,. \tag{11}$$

Determining the ratio W_t/W from formula (11), we obtain an expression for the selectivity in terms of the quantities measured in the experiment:

$$S = \frac{W_t}{W} = \frac{C_p(1 - C_f)}{(1 - C_p)C_f}\,. \tag{12}$$

The photoionization selectivity was studied for ^{176}Lu, ^{177}Lu, and ^{177m}Lu isotopes. The use of narrow atomic beams with a Doppler width of ~ 100 MHz suggests that the Doppler effect does not affect the photoionization selectivity.

As is clear from the diagram (see Fig. 6), the hyperfine structure of ^{176}Lu has the largest width (on the frequency scale) at all stages, and the extreme lines of the first transition ($5.5 \to 4.5$ and $8.5 \to 9.5$) are ~ 3 GHz away from the nearest lines of the dominant ^{175}Lu isotope. If the cross sections are equal in stages (see Table 5), the population of the main sublevel with $F = 8.5$ is 1.55 times higher, and, therefore, from the point of view of extraction, photoionization via $8.5 \to 9.5$ is preferable. The dynamic range of the mass spectrometer of ~ 300 limited the direct measurement of the ^{176}Lu photoionization selectivity to a level of 10^4. By way of indirect measurements, the photoionization selectivity of ^{176}Lu in the $8.5 \to 9.5 \to 8.5 \to 7.5$ channel was estimated at the level of $\sim 10^6$ at average DL intensities of 10 mW cm^{-2}, 10 mW cm^{-2}, and 3000 mW cm^{-2} at the stages.

Table 9. ^{177}Lu photoionization selectivity S for different channels [47].

^{177}Lu photoionization channel	Relative lower-sublevel population	C_{p177}*	S
$5 \to 6 \to 5 \to 4$	0.34	0.80(2)	$1.2(2) \times 10^5$
$5 \to 5 \to 5 \to 4$	0.34	0.90(1)	$2.7(3) \times 10^5$
$4 \to 3 \to 4 \to 3$	0.28	0.92(1)	$3.4(5) \times 10^5$
$2 \to 3 \to 4 \to 3$	0.16	0.88(2)	$2.2(4) \times 10^5$
$4/2 \to 3^{**} \to 4 \to 3$	0.16/0.28	0.93(1)	$4.0(6) \times 10^5$

* $C_{p176} < 0.02$ for all channels.
** DL1 radiation frequency is set between lines $4 \to 3$ and $2 \to 3$.

The choice of selective channels for ^{177}Lu radionuclide photoionization is not so obvious. Based on studies of HFS (see Figs 4 and 5), five ^{177}Lu excitation channels were identified (Table 8). The frequency shifts relative to ^{175}Lu in all channels turned out to be similar and, on average, were 1.2 GHz, −0.6 GHz, and 0.2 GHz at the stages. The hyperfine structure of the ^{176}Lu isotope is different: nuclear spin $I = 7$, $\mu_{176} = 3.1692(45)\,\mu_N$ [37], and the nearest channels turned out to be shifted in frequency by 1–3 GHz in two or three stages simultaneously. With respect to the ^{177m}Lu isomer, channels $5 \to 6 \to 5 \to 4$ and $2 \to 1 \to 2 \to 3$ can be considered selective at the first stage, and channels $4 \to 3 \to 4 \to 3$, $2 \to 3 \to 4 \to 3$, at the second and third stages.

The ^{177}Lu photoionization selectivity was measured for five channels (Table 9) [47]. The target isotope concentration in the evaporation sample was $C_{f177} = (3.4 \pm 0.4) \times 10^{-5}$. Average DL intensities at the stages were 3 mW cm^{-2}, 3 mW cm^{-2}, and 2000 mW cm^{-2}. The DL2 and DL3 pulses were delayed by 20 ns relative to the first stage pulse. The ^{177}Lu photoion current signals in all ionization channels were comparable and corresponded to the region of photocurrent transition to the saturation mode (in light intensity). Selectivity for all channels averaged $S = 2.7(4) \times 10^5$. An example of recording the photoion mass spectrum in the course of selective ^{177}Lu photoionization in channel

Table 10. Selective ^{177m}Lu photoionization channels (in terms of HFS components)* [48].

^{177m}Lu photoionization channel	Ionization channel Line shifts in stages relative to ^{177m}Lu, MHz		
	^{175}Lu	^{176}Lu	^{177}Lu
12 → 13 → 13 → 12	4 → 5 → 5 → 4 −996; +1267; +237	8.5 → 8.5 → 8.5 → 7.5 −1110; +995; −932	4 → 5 → 5 → 4 −2167; +1885; +24
13 → 13 → 13 → 12	5 → 5 → 5 → 4 −852; +1267; +237	8.5 → 8.5 → 8.5 → 7.5 +1078; +995; −932	4 → 5 → 5 → 4 +20; +1885; +24
12 → 12 → 13 → 12	5 → 5 → 5 → 4 +1232; −3005; +237	6.5 → 7.5 → 8.5 → 7.5 +298; +2858; −932	5 → 5 → 5 → 4 +40; −2387; +24
10 → 10 → 10 → 11	3 → 2 → 2 → 3 −832; +880; +545	7.5 → 6.5 → 6.5 → 6.5 +1274; +1225; −3640	2 → 3 → 2 → 3 +103; −1110; +298
* Indicated for each scheme are nearest ^{175}Lu, ^{176}Lu, and ^{177m}Lu isotope excitation channels and frequency distances to ^{177m}Lu for all ionization stages.			

5 → 6 → 5 → 4 is shown in Fig. 12. For time-matched pulses, the photoionization selectivity for channel 5 → 6 → 5 → 4 was half, 0.6×10^5, which is attributable to the influence of two-photon processes in the first and second transitions [47]. The two-photon process intensity is determined by the difference between the energy of the second excited state and the sum of laser photon energies of the first and second stages. For the nontarget ^{175}Lu isotope in channel 5 → 6 → 5 → 4, the difference is ∼ 600 MHz with a frequency difference of 1192 MHz in the first transition, which has the following effect: when the laser pulses coincide in time, the photoionization probability for nontarget ^{175}Lu increases to a greater extent than for the target ^{177}Lu isotope with a reduction in selectivity.

The photoionization selectivity of the ^{177m}Lu isomer was determined for four channels (Tables 10 and 11) [48]. A sample of metallic lutetium was irradiated in a neutron flux of 1.4×10^{13} cm^{-2} s^{-1} for 49 days and then stored for two months. As a result, at the time of the experiments, the concentration of the isomer was $C_{f177m} = (1.2 \pm 0.1) \times 10^{-6}$. The measured ^{177}Lu to ^{177m}Lu activity ratio of (0.2 ± 0.03) corresponded to the ^{177}Lu concentration of $(1 \pm 0.2) \times 10^{-8}$, which made it possible to neglect the contribution of photoions of the main isotope to the photoion signal at a mass of 177. The average laser intensities at the stages were 6 mW cm^{-2}, 4 mW cm^{-2}, and 2500 mW cm^{-2}, respectively. The DL2 and DL3 pulses were delayed by 20 ns relative to DL1. The ^{177m}Lu photoion mass spectra for ionization channels 12 → 13 → 13 → 12 and 13 → 13 → 13 → 12 are shown in Fig. 13.

Table 11. ^{177m}Lu photoionization selectivity S for different photoionization channels [48].

^{177m}Lu photoionization channel	Relative lower-sublevel population F	$S \times 10^5$		
		$S_{rel\ 175}$	$S_{rel\ 176}$	S
12 → 13 → 13 → 12	0.34	7.5(5)	0.62(5)	5.5(5)
13 → 13 → 13 → 12	0.34	2.0(2)	0.32(2)	1.8(2)
12 → 12 → 13 → 12	0.28	2.4(2)	0.48(5)	2.2(2)
10 → 10 → 10 → 11	0.16	1.2(1)	0.17(2)	1.0(1)

The highest selectivity $S = 5.5(5) \times 10^5$ ($C_{p177m} = 0.4$) was obtained during photoionization via channel 12 → 13 → 13 → 12. The decrease in selectivity for channels 13 → 13 → 13 → 12 and 10 → 10 → 10 → 10 is most likely due to smaller shifts of the ^{175}Lu lines at the first stage. The reason for the relatively low selectivity in channel 12 → 12 → 13 → 12 with the largest isotopic shift of 1.23 GHz seems to be the following. Despite the fact that the MO of the DL oscillates mainly in one longitudinal mode (single-mode lasing), there is a possibility of the appearance of weak lasing in the side (neighboring) modes. The frequency distance between the longitudinal modes is determined by the length

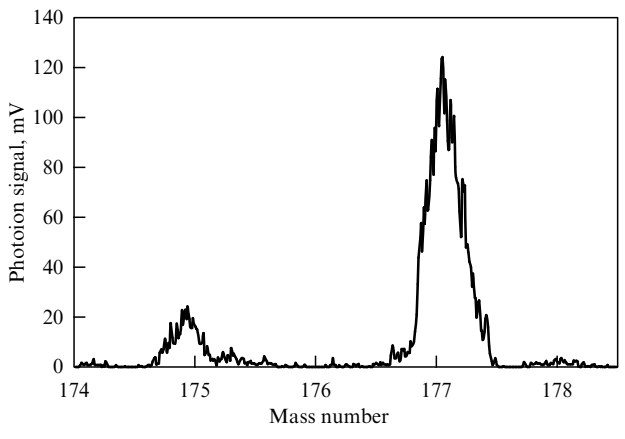

Figure 12. ^{177}Lu photoion mass spectrum in photoionization via channel 5 → 6 → 5 → 4 [47].

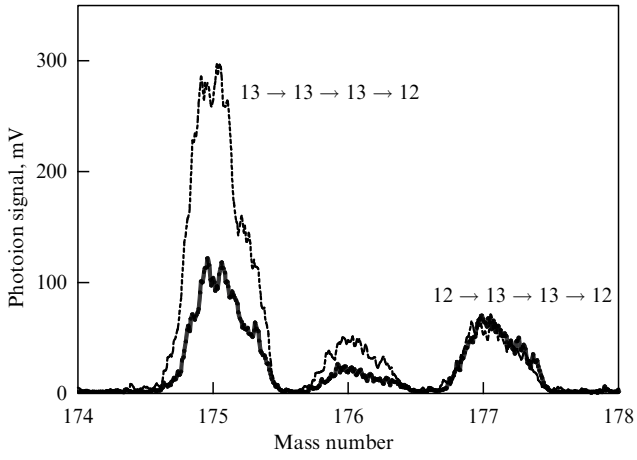

Figure 13. ^{177m}Lu photoion mass spectrum in photoionization via channels 12 → 13 → 13 → 12 and 13 → 13 → 13 → 12 [48].

of the resonator and, in our case (110–140 mm), lies in the range of 1100–1360 MHz. Obviously, the approach of the side mode to the frequency of the $12 \rightarrow 12$ nontarget isotope transition affects the selectivity of the process and can become especially noticeable under conditions of low isomer content. Judging by the spectral profile of the laser line, a decrease in selectivity is possible already when the side modes account for 10^{-4} of laser power.

A sharp (two orders of magnitude) decrease in the ^{177m}Lu photoionization selectivity due to the influence of two-photon processes was observed for time-coincident pulses. Due to the low content of the isomer, the selectivity in this case could only be measured for channel $12 \rightarrow 13 \rightarrow 13 \rightarrow 12$: it was $S = 6 \times 10^3$.

Here, a remark is in order: to achieve a high level of photoionization selectivity according to this scheme, it is necessary to pay special attention to the radiation parameters of the DL of the third stage, namely, to the level of the background component: DL radiation always contains amplified spontaneous emission (ASE), which is nonselective in frequency. Despite the fact that the ASE level of pulsed DLs, as a rule, does not exceed a few percent and is emitted in a wide spectral range of dye fluorescence (several tens of nanometers), its effect on selectivity can sometimes become noticeable. As found in Ref. [49], the ASE of DL3 leads to the involvement in the ionization process of nontarget isotopes from the lower metastable level $5d6s^2\ ^2D_{5/2}$ (1993 cm^{-1}) (see Fig. 2), the high intensity of this process being due to the following factors:

— appreciable metastable level population of 0.25 (at a lutetium evaporation temperature of 1700 °C);

— coincidence of the fluorescence maximum of the DL3 dye (Sulforhodamine 640) with the 6055 Å line arising from the $5d6s^2\ ^2D_{5/2} \rightarrow 5d6s6p\ ^4F^0_{5/2}$ transition;

— increased level of ASE during DL operation at the edge of the dye lasing range (618 nm);

— requirement for a high power level of the DL of the last stage (photoionization).

Careful filtering of the DL MO emission spectrum carried out in Ref. [49] made it possible to effectively reduce the ASE of the third stage DL, suppress the capture of nontarget isotopes, and improve the selectivity of the process by a factor of 20–40.

8. Production of weight quantity of ^{176}Lu

The production of ^{176}Lu isotope weight quantity was performed using a separating cell designed to separate neodymium isotopes [46]. Evaporator *1* (Fig. 14a) formed a flow of lutetium atoms of natural isotope composition with a length of 30 cm along the laser beam with collimation (limitation to 45° of the total angle of atomic expansion) in the transverse and longitudinal directions. On one side of the flow, in the shadow of the water-cooled shield *2*, there was a photoion collector *3*, and on the other side, deflector *4*, which served to increase and equalize the electric field strength. Two versions of the working volume were used in the experiments:

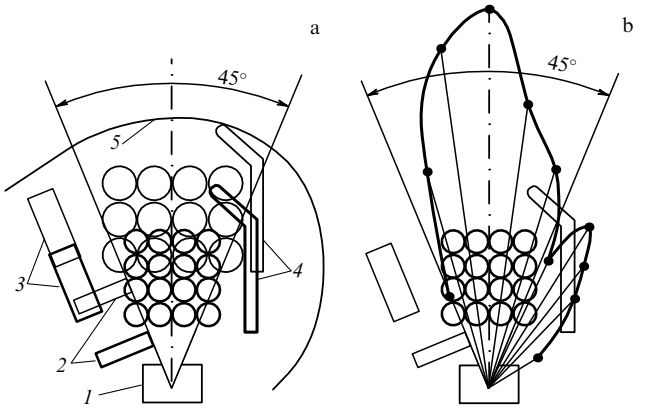

Figure 14. (a) Working volume: *1* — evaporator, *2* — water-cooled collector protection, *3* — photoion collector, *4* — deflector, *5* — dump control plate. Version 1 with laser beams 20 mm in diameter (bold lines). Version 2 with laser beams 30 mm in diameter (thin lines). (b) Angular distribution of the atomic flux obtained from an analysis of plates *5*.

the first one used laser beams 20 mm in diameter (bold lines), while the second made use of laser beams 30 mm in diameter (thin lines) and increased the width of the working volume and distance to the crucible. The optical multipass system provided multiple passes of the laser beam in the working volume to ensure efficient irradiation of evaporated atoms in the collimation sector. The evaporation rate was monitored using a quartz sensor, whose data were calibrated according to the deposition analysis data on plates *5* located above the working volume. Figure 14b displays the angular flow distribution obtained from an analysis of deposition on plates *5*.

Photoionization was carried out via the channel $8.5 \rightarrow 9.5 \rightarrow 8.5 \rightarrow 7.5$. The tuning of wavelengths to the ^{176}Lu isotope was controlled in a mass spectrometric setup, where a small part of the laser beam was directed. The powers were chosen in such a way that the intensities of laser radiation in the separation cell and in the interaction region in the mass spectrometer coincided for all three stages. The concentration of ^{176}Lu photoions in the mass spectrometer, averaged over the operating time (3–4 h), was 97%.

The total productivity was $p = 3.5$ mg h^{-1} at a ^{176}Lu concentration $C_p = 61\%$ in the first version and $p = 3.9$ mg h^{-1} at a ^{176}Lu concentration $C_p = 68\%$ in the second version (Table 12). The feed flow f according to the analysis of witness plates *5* was 4.1 and 4.6 g h^{-1} in the first and second versions, respectively, which makes it possible to determine the extraction degree K_{extr} of the target isotope, which is about 2%. At the same time, isotopic analysis of plates *5* in a narrow area above the centers of laser beams gives an ^{176}Lu concentration in the dump $C_w = 2.33\%$ and $C_w = 2.28\%$ in the first and second versions (natural concentration of 2.59%), which corresponds to the extraction degrees of 10% and 12% (see Table 12). Such a significant difference is attributable to the fact that the irradiation probability remains high for atoms passing in the

Table 12. Installation productivity indicators.

Beam diameter, mm	p, mg h^{-1}	C_p	f, mg h^{-1}	C_f	K_{extr}	$C_w^{\max}$	$K_{\text{extr}}^{\max}$
20	3.5	0.61	4100	0.0259	0.020	0.0233	0.10
30	3.8	0.68	4600	0.0259	0.022	0.0228	0.12

Table 13. Flux of neutral atoms to the collector.

Beam diameter, mm	$C_{\text{photo}}^{\min}$	$C_{\text{photo}}^{\max}$	$(I_{\text{ion}}/D)^{\max}$	$(I_{\text{ion}}/D)^{\min}$	$I_{\text{ion}}^{\min}$, mg h^{-1}	$I_{\text{ion}}^{\max}$, mg h^{-1}	$D^{\min}$, mg h^{-1}	$D^{\max}$, mg h^{-1}
20	0.68	0.97	8.3	1.6	2.2	3.1	0.37	1.3
30	0.72	0.97	16.4	2.3	2.7	3.7	0.22	1.2

region of the center of the rays. For atoms falling between the circumferences of the beam spots, the probability of irradiation is lower. In addition, sputtering of the previously produced product on the collector leads to a decrease in the recovery factor due to bombardment with photoions with an extraction voltage energy of 1–3 kV, which is confirmed by the presence of a slight enrichment in the isotope ^{176}Lu ($\sim 2.7\%$) on plates *5* in the area opposite the collector. The reduction in extraction degree in the separation cell to 10–12% compared to that achieved in experiments with a narrow beam $(17 \pm 3)\%$ is explained by the influence of the Doppler effect, when the frequency of laser radiation shifts and goes out of resonance for an atom flying at an angle to the vertical.

The concentration of ^{176}Lu in different places on the collector ranged from 37.3% on the surface to 72% downward, which indicates a noticeable flow of neutral atoms to the collector due to scattering in the working volume and on structural elements. To determine the actual values of the flux of neutral atoms, information is required on the isotopic composition of photoions in the working volume, which may differ from that measured in the mass spectrometer due to the Doppler effect in view of the fact that the angle of motion of atoms along the laser beam can reach 22.5° from the vertical, while in the mass spectrometer this angle is limited to 1.5°. In Ref. [46], the isotopic composition of neodymium photoions was determined using data for a number of even nontarget isotopes, each of which has one isolated absorption line. In the case of lutetium, each isotope has a pronounced hyperfine structure, and such a determination is impossible. Table 13 shows the maximum and minimum values of the flux of neutral atoms D and the photoion flux I_{ion}. Their determination was based on the fact that the ^{176}Lu photoion concentration C_{photo} in the working volume cannot be higher than in the mass spectrometer (97%) or lower than the maximum ^{176}Lu concentration on the product collector (68% for the first version and 72% for the second).

The results suggest that the extraction coefficient is somewhat higher in the second version of the working volume with laser beams 30 mm in diameter. This may be due to the higher uniformity of the laser beams and the higher quality of bringing into coincidence the beams of three photoionization stages with different wavelengths. The flow of neutral atoms to the collector in the second version turns out to be noticeably lower, because, in this case, the size of the working volume is larger, and in combination with approximately the same feed flow this leads to a decrease in the scattering of atoms in the working volume due to a decrease in their density.

The second version with a beam diameter of 30 mm is preferable when scaling the production by increasing the length of the working volume along the laser beam. The disadvantage of the second version is that its implementation requires an output laser power that is 2.3 times higher than for the first version.

9. Conclusions

To solve the problem of obtaining the ^{177}Lu medical radionuclide by laser photoionization isotope separation with tunable dye lasers pumped by copper vapor lasers, a three-stage lutetium photoionization scheme was found. For all levels of the scheme, we studied the hyperfine structure of the levels of the ^{175}Lu, ^{176}Lu, ^{177}Lu isotopes and the ^{177m}Lu isomer, which are important for solving the problem. Despite small isotopic shifts, for each isotope and isomer there are individual HFS components, which make it possible to achieve a high photoionization selectivity. The scheme found allows the following processes to be carried out:

(1) selective photoionization of the ^{176}Lu isotope for subsequent use to directly obtain the ^{177}Lu radionuclide;

(2) selective photoionization of ^{177}Lu for extracting the radionuclide from the irradiated material;

(3) selective photoionization of the ^{177m}Lu isomer to make an in-hospital autonomous generator of the ^{177}Lu radionuclide.

The photoionization scheme has a large photoionization cross section ($\sim 10^{-14}$ cm^2), which makes it possible to use low-power lasers (~ 10 W) and achieve significant extraction degrees of the target isotope (isomer) due to photoionization (10%–17%).

Acknowledgements. This study was supported by a grant from the Russian Science Foundation (project no. 17-13-01180) in regard to the extraction of radioactive isotopes of lutetium and a grant from the Russian Foundation for Basic Research (project no. 20-21-00019) in regard to analyzing the operation of a separation cell.

References

1. NuDat 3.0. National Nuclear Data Center. Brookhaven National Laboratory, https://www.nndc.bnl.gov/nudat2/
2. Toporov Yu G et al., Report on the 1st Research Coordination Meeting on "Development of Therapeutic Radiopharmaceuticals Based on 177Lu for Radionuclide Therapy", 4–8 December 2006, IAEA Headquarters, Vienna, Austria (Vienna: IAEA, 2006) p. 152
3. Banerjee S, Pillai M R A, Knapp F F *Chem. Rev.* **115** 2934 (2015)
4. Pillai M R A et al. *Appl. Radiat. Isotop.* **59** 109 (2003)
5. Park H et al. *J. Nucl. Sci. Technol. Suppl.* **45** (sup6) 111 (2008)
6. Bhardwaj R et al. *Sci. Rep.* **7** 44242 (2017)
7. Andreev B M et al, in *Izotopy: Svoistva, Poluchenie, Primenenie* (Isotopes: Properties, Production, Application) Vol. 1 (Ed. V Yu Baranov) (Moscow: Fizmatlit, 2005) p. 357
8. Letokhov V S *Sov. Phys. Usp.* **29** 70 (1986); *Usp. Fiz. Nauk* **148** 123 (1986)
9. Karlov N V et al. *Sov. Phys. Usp.* **22** 220 (1979); *Usp. Fiz. Nauk* **127** 593 (1979)
10. Letokhov V S, Moore C B *Sov. J. Quantum Electron.* **6** 129 (1976); *Kvantovaya Elektron.* **3** 248 (1976)
11. Tkachov A N, Yakovlenko S I *Quantum Electron.* **26** 839 (1996); *Kvantovaya Elektron.* **23** 860 (1996)
12. D'yachkov A B et al. *Quantum Electron.* **42** 953 (2012); *Kvantovaya Elektron.* **42** 953 (2012)
13. D'yachkov A B et al. *Appl. Phys. B* **121** 425 (2015)

14. Henkelmann R, Hey A, Buck O, in *Workshop* "*Physics for Health in Europe*" (Geneva: CERN, 2010)
15. Andreev O I et al. *Quantum Electron.* **36** 84 (2006); *Kvantovaya Elektron.* **36** 84 (2006)
16. Gadelshin V et al. *Hiperfine Interact.* **238** 28 (2017)
17. Gadelshin V et al. *Radiochim. Acta* **107** 653 (2019)
18. Fedosseev V N, Kudryavtsev Yu, Mishin V I *Phys. Scr.* **85** 058104 (2012)
19. Wendt K et al. *Fresenius J. Anal. Chem.* **364** 471 (1999)
20. Littman M G *Appl. Opt.* **23** 4465 (1984)
21. Grigoriev I S et al. *Proc. SPIE* **5121** 411 (2003)
22. D'yachkov A B et al. *Instrum. Exp. Tech.* **61** 548 (2018); *Prib. Tekh. Eksp.* (4) 81 (2018)
23. Ralchenko Y, Kramida A E, Reader J "NIST ASD Team NIST Atomic Spectra Database (Version 5)", https://www.nist.gov/pml/atomic-spectra-database
24. Meggers W F, Corliss C H, Scribner B F *Tables of Spectral-Line Intensities Arranged by Elements* (NBS Monograph 145, Pt. 1) (Washington, DC: National Bureau of Standards, 1975)
25. Smith P L et al. "Atomic spectral line database from CD-ROM 23 of R.L. Kurucz (2017)", https://www.cfa.harvard.edu/amp/ampdata/kurucz23/sekur.html
26. Suryanarayana M V *J. Opt. Soc. Am. B* **38** 353 (2021)
27. Suryanarayana M V, Sankari M *Sci. Rep.* **11** 18292 (2021)
28. Suryanarayana M V, Sankari M *J. Opt. Soc. Am. B* **38** 3331 (2021)
29. Rath A D, Biswal D, Rundu S *J. Quant. Spectrosc. Radiat. Transf.* **270** 107696 (2021)
30. Woodgate G K *Elementary Atomic Structure* (Oxford: Oxford Univ. Press, 1989)
31. D'yachkov A B et al. *Opt. Spectrosc.* **125** 839 (2018); *Opt. Spektrosk.* **126** 103 (2019)
32. D'yachkov A B et al. *Opt. Spectrosc.* **128** 6 (2020); *Opt. Spektrosk.* **128** 10 (2020)
33. Nunnemann A, Zimmermann D, Zimmermann P *Z. Phys. A* **290** 123 (1979)
34. Zimmermann D et al. *Z. Phys. A* **295** 307 (1980)
35. Georg U et al. *Eur. Phys. J. A* **3** 225 (1998)
36. Petersen F R, Shugart H A *Phys. Rev.* **126** 252 (1962)
37. Brenner T et al. *Nucl. Phys. A* **440** 407 (1985)
38. Heilig K, Steudel A *Atom. Data Nucl. Data Tabl.* **14** 613 (1974)
39. Witte S et al. *Eur. Phys. J. D* **20** 159 (2002)
40. Jin W G et al. *Phys. Rev. A* **49** 762 (1994)
41. Persson J R *Atom. Data Nucl. Data Tabl.* **99** 62 (2013)
42. Fedchak J A et al. *Astrophys. J.* **542** 1109 (2000)
43. D'yachkov A B et al. *Opt. Spectrosc.* **128** 289 (2020); *Opt. Spektrosk.* **128** 301 (2020)
44. Axner O et al. *Spectrochim. Acta B* **59** 1 (2004)
45. Dyachkov A B et al. *Quantum Electron.* **48** 1043 (2018); *Kvantovaya Elektron.* **48** 1043 (2018)
46. Babichev A P et al. *Quantum Electron.* **35** 879 (2005); *Kvantovaya Elektron.* **35** 879 (2005)
47. Ageeva I V et al. *Quantum Electron.* **49** 832 (2019); *Kvantovaya Elektron.* **49** 832 (2019)
48. D'yachkov A B et al. *Quantum Electron.* **51** 317 (2021); *Kvantovaya Elektron.* **51** 317 (2021)
49. D'yachkov A B et al. *Quantum Electron.* **46** 574 (2016); *Kvantovaya Elektron.* **46** 574 (2016)
50. Kuhnert A, Nunnemann A, Zimmermann D *J. Phys. B* **16** 4299 (1983)